

Investigation on space charge and charge trap characteristics of gamma-irradiated epoxy micro–nano composites

eISSN 2397-7264

Received on 25th July 2019

Revised 10th October 2019

Accepted on 28th October 2019

E-First on 6th February 2020

doi: 10.1049/hve.2019.0188

www.ietdl.org

Myneni Sukesh Babu¹, Ramanujam Sarathi¹ ✉, Nilesh Jayantilal Vasa², Takahiro Imai³

¹Department of Electrical Engineering, Indian Institute of Technology Madras, Chennai 600036, India

²Department of Engineering Design, Indian Institute of Technology Madras, Chennai 600036, India

³Toshiba Corporation, Power, and Industrial Systems R&D Centre, 1, Toshiba-cho, Fuchu-shi, Tokyo 183–8511, Japan

✉ E-mail: rsarathi@iitm.ac.in

Abstract: Epoxy nano–micro composite specimen prepared with micro silica and ion trapping nanoparticle, by shear mixing process, was exposed to gamma radiation and its performance for space charge and charge trap characteristics were analysed. The threshold for space charge accumulation of epoxy nanocomposites reduces and rate of space charge accumulation increases with an increase in dosage of gamma irradiation. The average growth of space charge density during poling and charge decay rate during depoling are relatively higher for gamma-irradiated specimens than the virgin specimen. The initial surface potential has a marginal reduction with increase in the dosage of gamma radiation, but the surface potential decay rate has increased significantly. Trap distribution characteristics indicate more number of shallow traps and increase in charge mobility after irradiation. The relative permittivity and loss tangent of the specimens have high impact due to gamma irradiation. The activation energy calculated from DC conductivity by Arrhenius law reduces with increment in radiation dose. Laser-induced breakdown spectroscopy reflected no change in elemental composition with gamma-irradiated specimen. The variation in plasma temperature and ion line to atomic line intensity ratio with dosage of gamma radiation have direct correlation to the Vickers hardness number of the specimens.

1 Introduction

Polymer nanocomposite materials especially epoxy nanocomposites are gaining importance to use as an insulant in power apparatus like dry-type transformers, rotating machines, as spacers in GIS and in cable joints because of their improved properties such as high breakdown strength, high volume resistivity and low dielectric loss [1–5]. The surface of the nanofiller being highly active, it is possible to achieve desired electrical and mechanical properties of insulating material by adding small amount of nano and micron-sized fillers to the base epoxy matrix [5–11]. Tsekmes *et al.* have indicated that nano–micro composites have superior electrical and thermal properties. It is an industrial practice to use 60–70 wt.% of micron-sized silica as filler in epoxy-based insulating material [12, 13]. Imai *et al.* have stated that silica micro fillers have lower thermal expansion coefficient [14]. Mishra *et al.* studied water droplet initiated discharge studies with ion-trapping agent IXEPLAS® (hydrotalcite compound modified with zirconium phosphate) filled epoxy nanocomposites [15]. Inorganic ion exchangers (such as zirconium phosphate) have high oxidation resistance with good ion trapping properties and thus they can be used in the insulation structure to improve its reliability [16]. The IXE nanoparticles can acquire the ionic compounds formed due to ageing of insulating material causing reduction in resistivity of the insulation materials. Also, the composition of IXE material includes zirconium, which is a refractory material, can enhance the thermal capability of the insulating material. The study on the impact of adding inorganic ion exchangers to epoxy micro composites, to use them as an insulating material, is very limited. It is essential to understand the impact of gamma irradiation to the epoxy nanocomposites with IXE nanofillers included, where the database needs to be generated.

The use of epoxy insulating materials in radiation environments such as nuclear power plants and space equipment is increasing rapidly. Here, it is essential to understand the epoxy nanocomposites performance with different levels of irradiation with gamma rays. These ionising radiations can alter the molecular

structure of polymeric insulating materials through mechanisms like chain scissions, cross-linking and oxidation. The structural changes that are induced due to the exposure of gamma radiation can possibly alter the charge trap characteristics, hence resulting in the change in behaviour of the surface as well as bulk charge characteristics of insulating material [17]. Hence, it is necessary to understand the effect of gamma radiation on the surface potential and charge trap characteristics of epoxy micro–nano composites. Surface potential measurement is a simple and low-cost technique, which allows one to understand various physical processes including polarisation, charge injection and surface conduction process, in an insulating material [18, 19].

One of the major problems associated with the polymeric insulating materials is their tendency to accumulate space charge under high electric fields, especially in high voltage DC applications [20–22]. Chen *et al.* have stated that the effect of gamma radiation on the space charge of the insulating material depends on the dosage of the radiation and also on the ambience of radiation [23]. Voltage polarity reversal phenomenon in general happens in HVDC transmission systems for achieving bi-directional power flow. The presence of space charge during the voltage polarity reversal can become a vital threat to the insulation cables in HVDC system [24]. So, it is essential to understand the influence of gamma radiation on the space charge under different voltage polarities and during polarity reversal.

High energy ionising radiations can alter the dielectric behaviour of the insulating material. Also, the dielectric constant depends on the temperature of the insulating material. Laghari and Hammoud have studied the effect of radiation on polymer dielectrics and indicated that exposure to radiation can result in the deterioration of the dielectric properties of the polymeric insulating material [25]. So, the gamma-irradiated specimens need to be characterised by dielectric response spectroscopy (DRS) at different temperatures.

Laser-induced breakdown spectroscopy (LIBS) can be used as a testing tool to find the elemental composition and also the level of ageing of the insulating material [26, 27]. It is one of the prominent techniques for the estimation of hardness of the material, just by

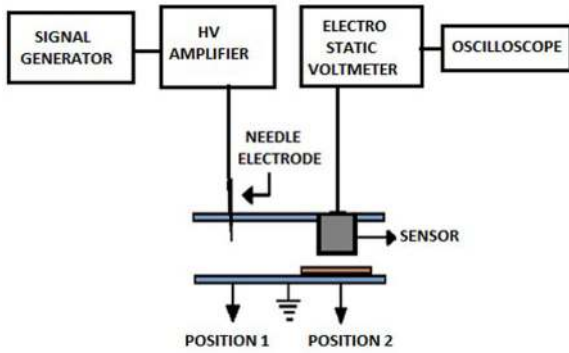


Fig. 1 Surface potential measurement setup

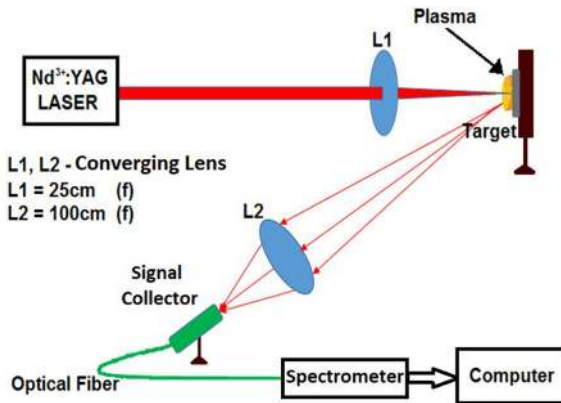


Fig. 2 Experimental setup of LIBS study

shining laser on the specimen. Aberkane *et al.* have correlated plasma temperature calculated through LIBS and the hardness of the material [28]. In this study, an attempt has been made to understand the plasma temperature and the hardness of the material with the level of gamma irradiation.

Having known all these aspects, to understand the impact of gamma irradiation to epoxy nanocomposites, the following methodical experimental studies need to be carried out to understand its performance. (i) The effect of gamma radiation on the space charge accumulation characteristics of the epoxy micro-nano composites through pulsed electro acoustic (PEA) measurement studies. (ii) The surface potential decay characteristics and charge trap characteristics of the test specimens. (iii) The variation in dielectric parameters of the gamma-irradiated epoxy nanocomposites at different frequencies. (iv) LIBS analysis for understanding the change in the emission spectra and plasma temperature of nanocomposite material due to gamma-ray irradiation.

2 Experimental studies

2.1 Sample preparation

The specimen used for the study is an epoxy micro-nano composite, which contains base epoxy resin filled with crystalline SiO₂ micro particle (of 66 wt. %) and ion trapping nanoparticle (0.7 wt. %). The IXE nanoparticles and the crystalline SiO₂ micro fillers were obtained commercially. The IXE nanoparticles are 200–500 nm in diameter. Moreover, the crystalline SiO₂-fillers of average diameter of 14 μm are used for the study. In general, surface modification by silane coupling agent is broadly-divided into two methods, pre-treatment and in-situ method. In this study, in-situ method is adopted by mixing the epoxy resin, hardener, SiO₂-fillers, IXE nanoparticles and silane coupling agent together. Standard shear mixing, degassing, casting and curing procedures were followed in the preparation of epoxy micro-nano composite specimens [15]. The epoxy micro-nano composite material is subjected to gamma radiation through a ⁶⁰Co radiation source in air

ambience with a dosage rate of 660 Gy/h up to total doses of 4 and 8 kGy.

2.2 Space charge measurement

Techimp PEA Flat System is used for space charge measurement. The complete PEA Flat System used here consists of a PEA Flat cell, a high voltage variable DC source in the range of 0–30 kV, a voltage pulse generator 0–500 V, a DC source of 18–24 V, to supply the amplifiers in the cell and an oscilloscope (Tektronix, 350 MHz, 5 GS/s). In this method, a pulsed voltage is applied across the sample. The charges that are stimulated by the applied pulsed electric field, experience a perturbation force that travels in the form of pressure waves along the direction of the applied pulse signal. These waves are converted into electric signals by a poly vinylidene fluoride piezoelectric transducer. The electric signals after passing through an amplifier, can be recorded with the help on the oscilloscope. The test specimen used here is a flat type sheet material with dimensions 40 × 40 × 1 mm³.

2.3 Surface potential measurement

Needle plane configuration of electrodes was used in the surface potential measurement setup to spray charges on the insulating material by generating corona at 10 kV positive and negative DC voltages using a high voltage amplifier (Trek model 20/20 C). An electrostatic voltmeter (Trek model 341B) was used to measure the surface potential. In Fig. 1, when the sample was at position 1, the charges were sprayed on top of the test specimen, and at position 2, the surface potential developed was measured by using electrostatic voltmeter.

2.4 Dielectric response spectroscopy

DRS is performed to characterise the fundamental dielectric properties of the material at different frequencies and different temperatures. DRS was performed by using Novocontrol technology broadband dielectric/impedance spectrometer (Alpha-A high performance frequency analyser). The test specimens were cut into 20 mm diameter circles for dielectric response studies. The dielectric response studies were carried out in the frequency range of 0.1–10⁶ Hz at different temperatures ranging from –50 to 110°C.

2.5 Laser-induced breakdown spectroscopy (LIBS)

In LIBS, a pulsed laser is focused on the sample to create a plasma on the surface of the sample, which is created when the energy provided by the laser pulse is greater than that of the threshold fluence of the material. Then, electromagnetic radiations are emitted by the excited elements in plasma, while coming to the lower energy states. Wavelengths of these radiations are fingerprints of the elements that are present in the material. The experimental setup of LIBS is shown in Fig. 2. Here, an Nd³⁺ YAG laser is focused on the sample using 25 cm focal length lens. The optical emission is captured with the help of a 100 cm focal length lens and is passed to a spectrometer (Ocean Optics) through an optical fibre of core diameter 400 μm, 0.22 NA.

3 Results and discussion

3.1 Effect of gamma radiation on space charge characteristics of epoxy specimens

The mean magnitude of space charge density accumulated $q(E, t)$ in the specimen can be calculated as shown in the following equation [29]:

$$q(E, t) = \frac{1}{x_1 - x_0} \int_{x_0}^{x_1} |q_p(x, t; E)| dx \quad (1)$$

where x_0 and x_1 represent the position of the electrodes (induced charges at the electrodes are not taken into account), and $q_p(x, t; E)$ is the charge density at position x , time t and applied electric field

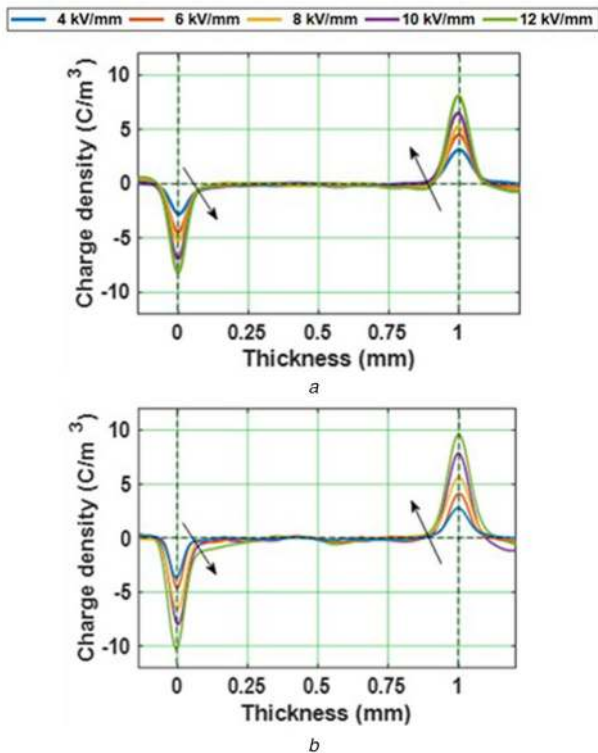


Fig. 3 Variation in space charge density under different applied electric fields in (a) Virgin and, (b) 8 kGy gamma-irradiated epoxy micro-nanocomposites

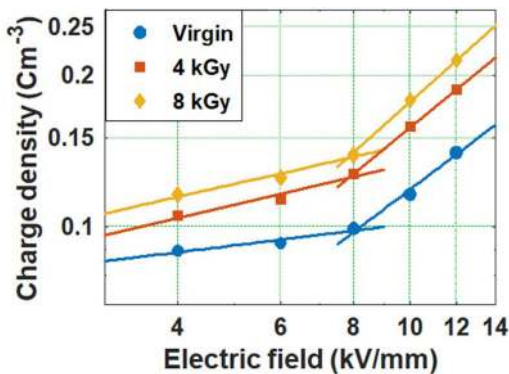


Fig. 4 Characteristic plot of average space charge density as a function of the applied electric field

E. The mean magnitude of charge density calculated across total thickness of the specimen L , gives an over-estimated value of charge density. In this study, to exclude the induced charges, involves in the consideration of lower and upper limits of the above integration as x_0 and x_1 , instead of 0 and L . By suitably selecting the positions of x_0 and x_1 , the exact value of charge density of accumulated charge in the bulk of the specimen were calculated.

Fig. 3 represents the space charge profiles of epoxy specimens under the application of various positive DC electric fields. Presence of homo-charge is observed near the vicinity of electrode–dielectric interface for the epoxy nanocomposites. The net space charge distribution will depend on the processes like charge injection/extraction and charge transportation. When the rate of charge injection is higher than the rate of charge transportation, it results in the formation of homo-charge. It is observed that the amount of homo-charge formed near the interface increases with increase in the magnitude of the electric field applied. The charge carriers near the electrode–dielectric interface need to overcome the potential barrier in order to enter into the dielectric material. Whenever the electric field is applied, the potential barrier is reduced, allowing the charge carriers into the material. This type of charge injection phenomenon is called as the

Table 1 Parameter values of virgin and gamma-irradiated specimens

Specimen	E_T , kV/mm	b , $\mu\text{CV}^{-1}\text{m}^{-2}$
Virgin	8.08	0.876
4 kGy	7.88	0.952
8 kGy	7.83	1.038

Schottky process [30]. With the increase in the magnitude of electric field applied, the potential barrier tends to decrease causing the charge injection easier. So, the amount of homo-charge formed near the interface increases with increase in the applied electric field.

The magnitude of space charge accumulated at an applied electric field is one of the significant factors in understanding the extent of degradation of the insulating material. The threshold for space charge accumulation (E_T) and the rate of space charge accumulation (b) can be calculated from average charge density versus applied electric field plot (Fig. 4). The parameters E_T and b are independent of electric field applied and the time, provided that the charge density is measured when the space charge accumulation reaches quasi-steady state condition [29]. At each applied electric field, average space charge density after one hour of poling time is taken into consideration for determining the threshold (E_T). For each specimen, the slope of the fitted line above the threshold point (E_T) in the average charge density versus applied electric field plot, as shown in Fig. 4, gives the rate of space charge accumulation [29]. The E_T and b for virgin and gamma-irradiated specimens are represented in Table 1. The parameter E_T is marginally higher for virgin specimen when compared to gamma-irradiated specimens, indicating that the field above which a significant accumulation of space charge occurs is decreasing with increase in dosage of gamma radiation. Also, the parameter b is increasing with increase in dosage of gamma radiation. This indicates the presence of more amount of charge accumulation in case of gamma-irradiated specimens when compared to virgin specimen, at higher electric fields. Thus, the reduction in E_T and increase in b with dosage of gamma irradiation is an indication for the possibility of early degradation of the insulating properties of the material resulting in premature breakdown.

Since the threshold for space charge accumulation is found to be around 8 kV/mm, the electric field of 10 kV/mm is selected for further analysis. The variation in the space charge profiles of epoxy specimens with respect to poling time, under the application of 10 kV positive DC voltage is represented in Fig. 5. It is observed that there is an increase in the homo-charge accumulation near the electrode–dielectric interface with respect to poling time. The charge accumulation near the vicinity of electrode–dielectric interface can be clearly seen from the space charge evolution plot as shown in Fig. 6. Fig. 7 represents the space charge distribution of test specimens at different instants of time during depoling. The induced charge at the electrode-specimen interface is decreased instantly just after reducing the applied voltage to zero, leaving behind the accumulated homo-charge.

The variation in average charge density of the epoxy specimens during poling and depoling period is represented in Fig. 8. The average space charge density is found to be higher in the case of gamma-irradiated specimens compared to virgin specimen (Fig. 8a). Chen *et al.* studied the space charge behaviour of gamma irradiated polyethylene material under different radiation environments and have observed an increase in the space charge accumulation in the gamma-irradiated specimens compared to virgin specimens irradiated in the presence of air, while only a small amount of charge accumulation is found in samples irradiated in both vacuum and nitrogen environment [23]. Similar characteristics are observed with epoxy-based insulating material, where the average space charge density increases with increase in the dosage of radiation in the presence of the air medium (Fig. 8a). Internal charge carriers (electrons or holes) are formed when they gain sufficient energy to escape from valence band to conduction

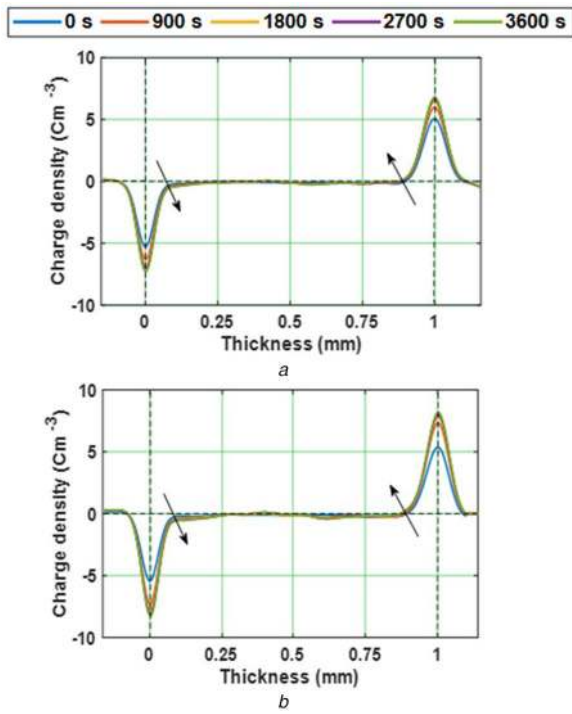


Fig. 5 Space charge distribution during poling in (a) Virgin and, (b) 8 kGy gamma-irradiated epoxy micro-nanocomposites under 10 kV positive DC voltage

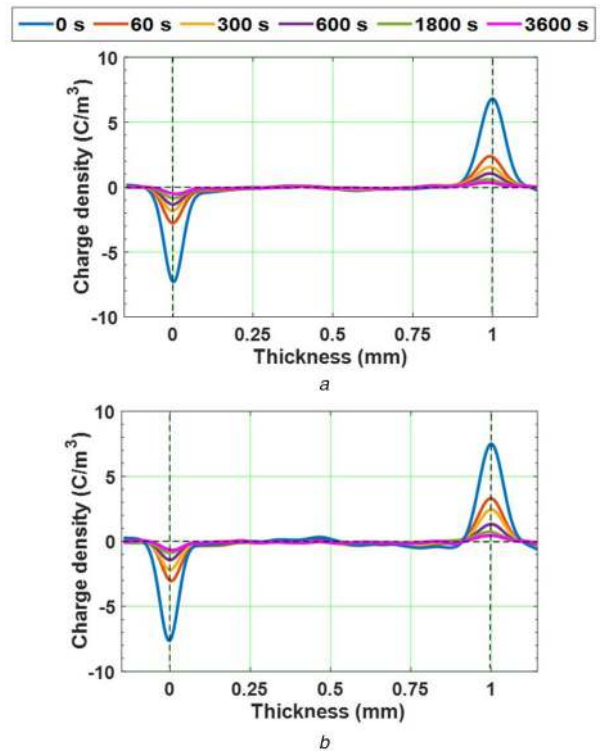


Fig. 7 Space charge distribution during depoling of (a) Virgin and, (b) 8 kGy gamma-irradiated epoxy micro-nanocomposites after reduction of 10 kV positive DC voltage

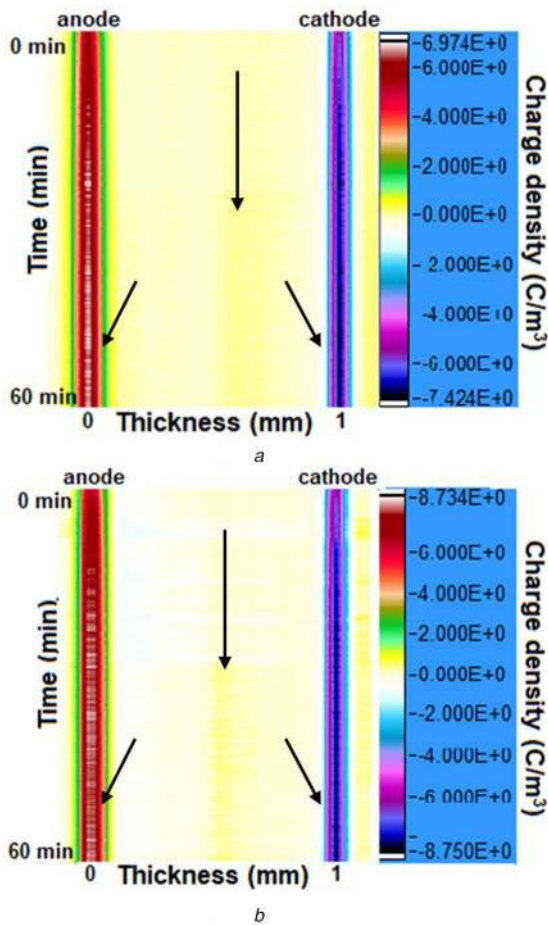


Fig. 6 Space charge evolution during poling of (a) Virgin and, (b) 8 kGy gamma-irradiated epoxy micro-nanocomposites under 10 kV positive DC voltage

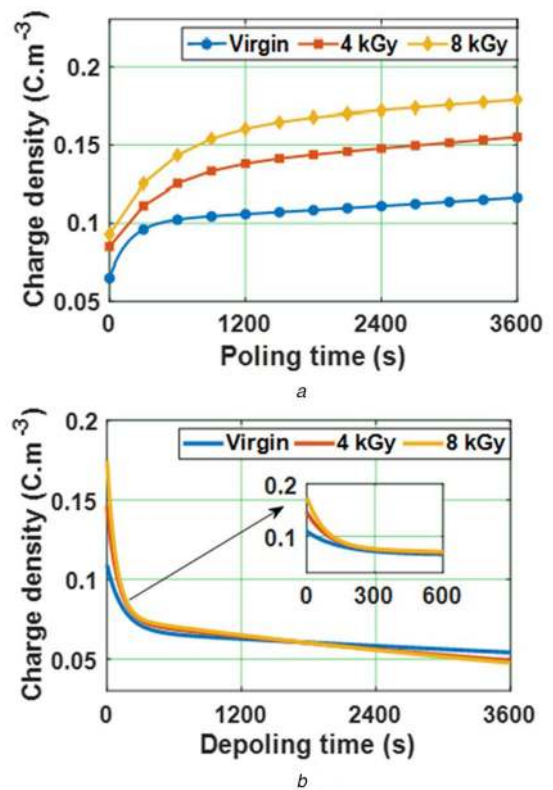


Fig. 8 Average space charge density of virgin and gamma-irradiated specimens during (a) Poling time and, (b) Depoling time

band. The excitation energy to the electrons can be obtained by various means like thermal, electrical or radio-active phenomenon. Thus, the cause for increase in space charge density in epoxy

nanocomposites could be due to the formation of internal charge carriers or free radicals in the bulk of the material during oxidation phenomenon, when exposed to gamma radiation.

Also, the charge decay rate during de-poling is more in the case of gamma-irradiated material when compared to virgin epoxy nanocomposites (Fig. 8b). Higher charge decay rate indicates that

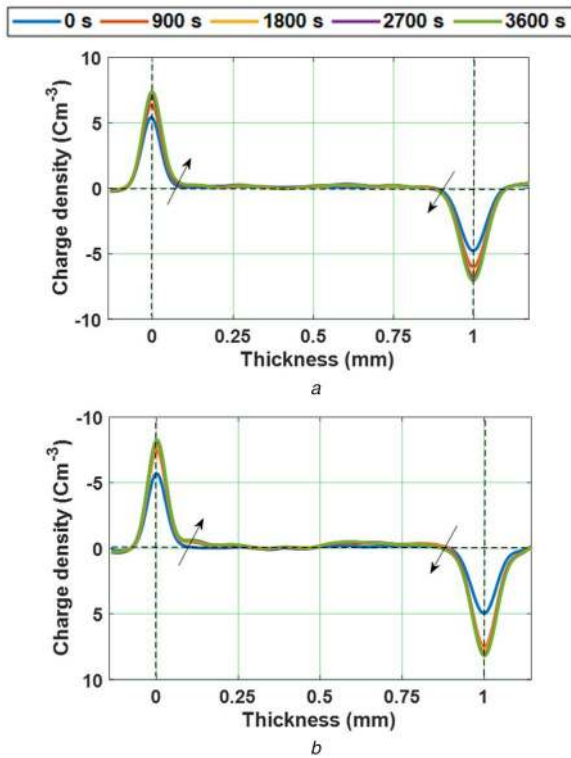


Fig. 9 Space charge distribution during poling in (a) Virgin and, (b) 8 kGy irradiated specimens under 10 kV negative DC voltage

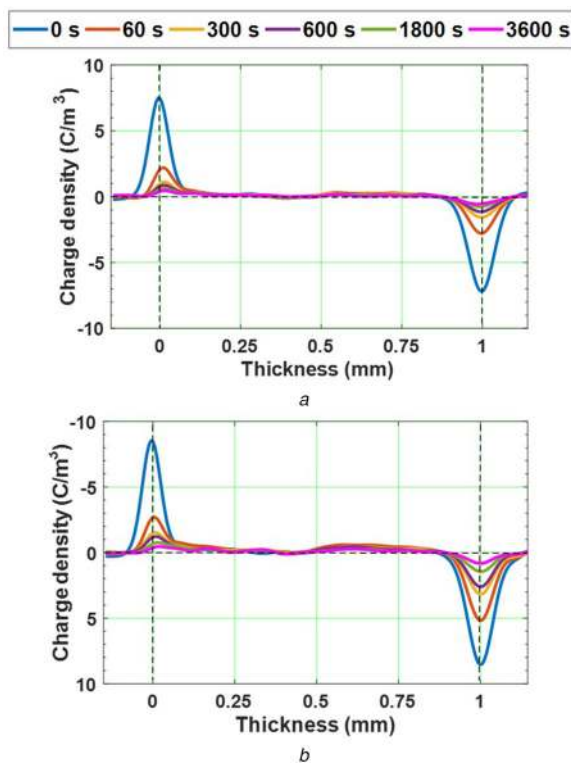


Fig. 10 Space charge distribution during depoling of (a) Virgin and, (b) 8 kGy irradiated epoxy specimens after reduction of 10 kV negative DC voltage

the rate of charge transportation in the bulk of the material is higher. The transportation of charge carriers depends on the depth of the trapping sites. Chen and Fu stated that the concentration of carbonyl groups increases with radiation dose and that the carbonyl groups generate a shallow trap that readily assists charge transport [31]. Thus, the faster decay of space charge in the gamma-irradiated specimens during de-poling could be due to the

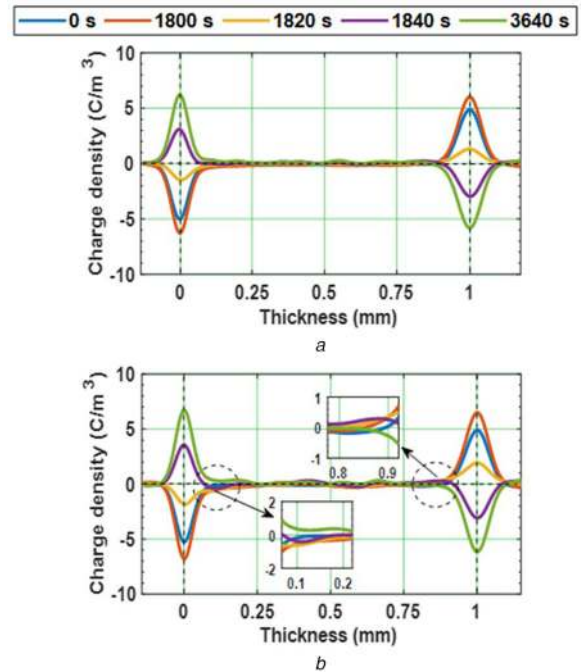


Fig. 11 Space charge distribution under polarity reversal from positive to negative DC field stress in (a) Virgin and, (b) 8 kGy gamma-irradiated specimens

formation of relatively more number of shallow traps which increases the rate of charge carrier transportation.

The space charge profiles of virgin and gamma irradiated epoxy nanocomposites under the application of negative DC stress of 10 kV/mm is shown in Fig. 9. Homo-charge accumulation due to charge injection is found near the vicinity of the electrode-dielectric interface. Similar to the case of positive DC field stress, the charge accumulation in epoxy nanocomposites just after the poling period of 3600 s is found to be higher in the case of gamma-irradiated specimens compared to virgin specimen. Fig. 10 represents the space charge distribution of test specimens at different instants of time during depoling, just after the removal of negative DC voltage.

To understand the effect of voltage polarity reversal, the epoxy nanocomposites are subjected to 10 kV/mm positive DC field for a poling time of 1800 s before the polarity reversal. The period of voltage polarity reversal is maintained as 40 s. After reversal, the specimens are subjected to negative DC stress of 10 kV/mm for a period of 1800 s. Figs. 11 and 12 represent the variation in space charge density and electric field distribution profiles of virgin and gamma-irradiated epoxy nanocomposites during poling time and polarity reversal with respect to time, respectively.

In Fig. 11b, the homo-charge accumulated before the polarity reversal (at 1800 s) is retained during voltage polarity reversal change (1800–1840 s). The modified field distribution due to this retained space charge will have an effect on the space charge distribution after a polarity reversal. After the polarity reversal, the space charge accumulated due to opposite polarity field stress, first reduces the retained charge, then cancels it and finally the space charge with reversed polarity is being accumulated at the same position at the end of poling period after reversal (at 3640 s). Wang *et al.* have observed the similar phenomenon in CB/LDPE composites and have concluded that the homo-charges injected will remain in the dielectric as hetero-charges after the polarity reversal to applied DC field. They also have indicated that a part of charge remained after polarity reversal could migrate under reversed field or get neutralised by the electrons injected from cathode [32]. A similar phenomenon is noticed here, which can be clearly observed from Fig. 11b, representing the space charge density of 8 kGy irradiated specimen during voltage polarity reversal.

The presence of space charge in a dielectric can lead to the field distortion, which results in the dielectric to experience higher electric fields in some regions than the applied electric field. The

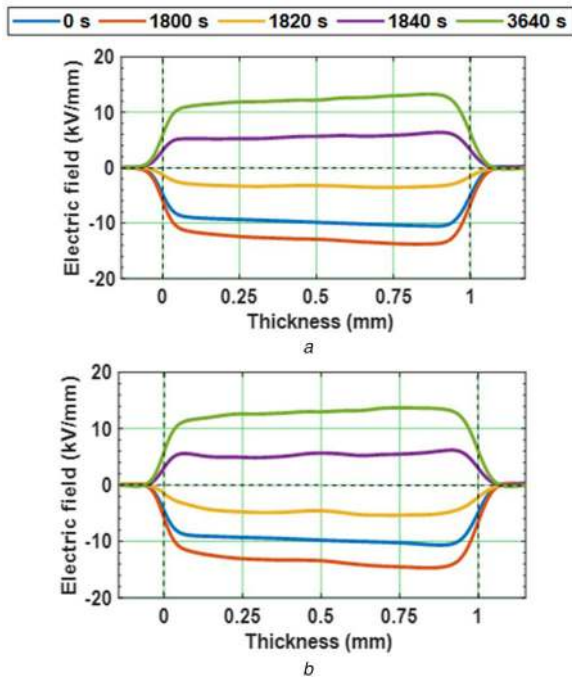


Fig. 12 Electric field distribution under polarity reversal from positive to negative DC field stress in (a) Virgin and, (b) 8 kGy gamma-irradiated specimens

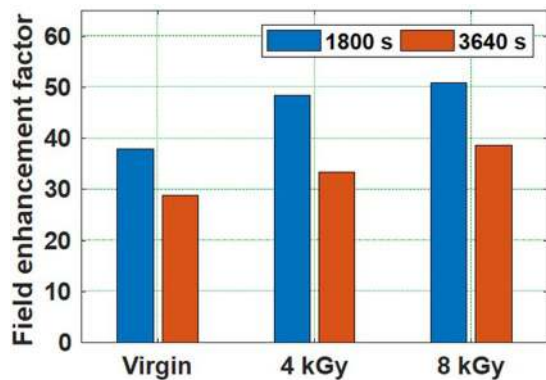


Fig. 13 Field enhancement factor of virgin and gamma-irradiated epoxy nanocomposites

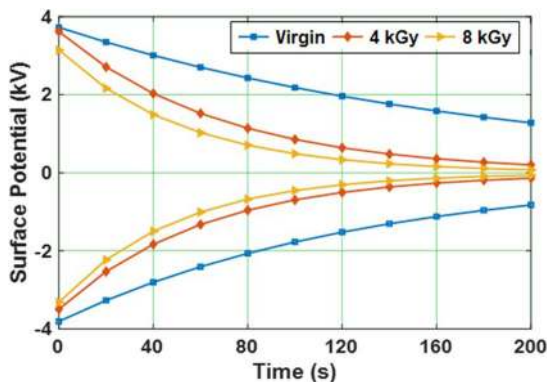


Fig. 14 Surface potential decay characteristics of virgin and gamma irradiated specimens under positive and negative DC corona charging

extent of field distortion can be determined using the field enhancement factor [33]. It can be expressed as shown in the following equation:

$$F = \frac{E - E_a}{E_a} \times 100 \quad (2)$$

Table 2 Initial potential and mean lifetime of virgin and gamma-irradiated specimens under positive DC corona

Sample	Positive DC		
	Initial potential, kV	Mean lifetime, s	Trap depth at peak of trap distribution, eV
Virgin	3727	187.09	1.001
4 kGy	3688	69.28	0.981
8 kGy	3145	53.56	0.976

Table 3 Initial potential and mean lifetime of virgin and gamma-irradiated specimens under negative DC corona

Sample	Negative DC		
	Initial potential, kV	Mean lifetime, s	Trap depth at peak of trap distribution, eV
Virgin	-3811	130.80	1.009
4 kGy	-3497	61.88	0.985
8 kGy	-3318	50.35	0.978

where F is the field enhancement factor (%), E_a is the applied electric field stress (kV/mm) and E is the maximum electric field in the bulk of the sample (kV/mm).

The field enhancement factor of virgin and gamma-irradiated epoxy nanocomposites just before polarity reversal (at 1800 s) and after a poling time of 1800 s from polarity reversal (at 3640 s) is shown in Fig. 13. It has been observed that the field enhancement is found to be increasing with increase in dosage of gamma radiation before and after the voltage polarity reversal of applied DC stress.

3.2 Surface potential decay and trap characteristics

The surface potential decay characteristics of test specimens under the application of positive and negative DC voltages are shown in Fig. 14. The surface potential decay characteristics have been approximated as an exponential pattern as shown in the following equation:

$$V(t) = V_0 e^{-\lambda t} \quad (3)$$

where V_0 is the initial surface potential accumulated and λ is the decay rate. The mean lifetime of the surface potential can be calculated by taking the inverse of the decay rate (λ).

The initial potential and mean lifetime (τ) of the virgin and gamma-irradiated epoxy specimens under positive and negative DC corona are represented in Tables 2 and 3. With the increase in the dosage of radiation, the magnitude of the initial potential is marginally reduced and the decay rate is increased significantly. The decay rate is mostly dependent on the energy level of surface traps that are altered by the radiation-induced degradation reactions like chain scission and oxidation [34]. The carbonyl and hydroxyl groups are the radiation induced reaction products that introduce shallow traps on the surface of the material. Presence of shallow traps results in the increase of carrier mobility of the surface charge, which tends to increase with the increase in the radiation dose. The surface potential decay characteristics of epoxy nanocomposites are high under negative DC voltage than under positive DC voltage. It is because of the higher mobility of negative ions when compared to positive ions, the decay rate is more when negative DC voltage is applied.

According to isothermal current decay theory [35], the surface charge distribution can be obtained from surface potential characteristics. The distribution function of electrons or holes is represented in the following equation:

$$N(E) = \frac{2 \epsilon_0 \epsilon_r}{q L^2 k T f_o(E)} t \frac{dV}{dt} \quad (4)$$

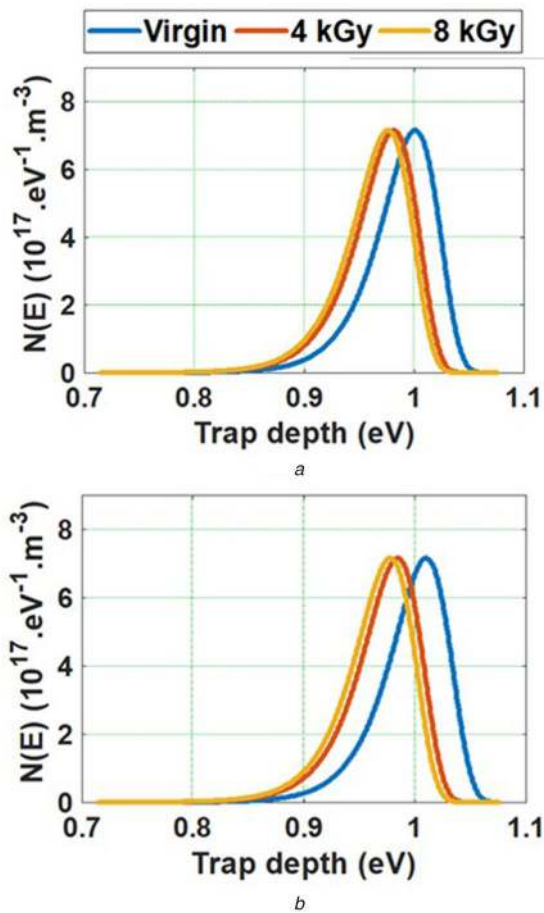


Fig. 15 Trap distribution characteristics of virgin and gamma irradiated specimens under (a) Positive DC and, (b) Negative DC corona charging

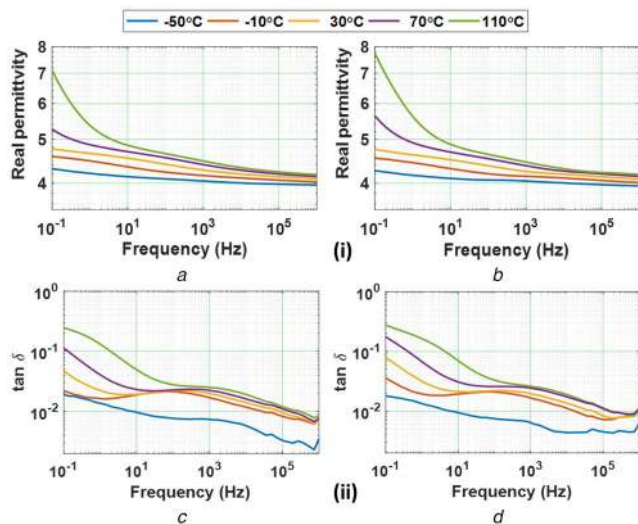


Fig. 16 Variation in (i) relative permittivity and (ii) $\tan \delta$ values of (a) Virgin and, (b) 8 kGy gamma irradiated specimens

where q is the electron charge, L is the thickness of the sample, k is Boltzmann constant, T is the absolute temperature, t is the time, and $f_0(E)$ is the initial electron occupancy rate.

The trap depth ΔE can be expressed as shown in the following equation:

$$\Delta E = E_C - E_M = kT \ln(\nu t) \quad (5)$$

where E_C is conduction band energy and E_M is the demarcation energy, k is the Boltzmann constant ($1.38 \times 10^{-23} \text{ m}^2 \text{ kg s}^{-2} \text{ K}^{-1}$), ν

is the escape frequency of electron (10^{12} Hz) and T is the absolute temperature [36].

Trap distribution was analysed according to (4) and (5). Fig. 15 represents the trap depth variation of virgin and gamma-irradiated epoxy composites at positive DC and negative DC corona and it varied in the range of 0.835–1.065 eV and 0.84–1.07 eV, respectively. The trap depth at the peak value of trap distribution characteristics of virgin and gamma-irradiated epoxy composites under positive DC and negative DC corona were represented in Tables 2 and 3. A reduction in the trap depth can be observed from the left shift in the peak value of trap distribution characteristics for the gamma-irradiated specimens compared to virgin specimen. This left shift in the peak value indicates the reduction of the energy barrier for charge detrapping. It also confirms that the charges get trapped in relatively shallow traps in the gamma-irradiated samples compared to virgin sample.

3.3 Dielectric response spectroscopy

Fig. 16 represents the frequency variation in real relative permittivity and dielectric loss tangent ($\tan \delta$) of epoxy nanocomposites at different temperatures ranging from -50 to 110°C . The real relative permittivity was found to be reduced with the increase in the frequency, in case of both virgin and gamma-irradiated samples. In epoxy specimens, the permittivity depends on the number of orientable dipoles present in the system and the capability of the dipoles to orient with the application of electric field [37, 38]. With low-frequency supply voltage, the functional groups with dipolar nature align in the direction of applied electric field, and results with higher permittivity. With the frequency of supply voltage increased, the polar entities like amines and hydroxyls formed from the ring-opening of epoxides by amines resist to respond with supply voltage frequency, thereby reducing the permittivity of the material [39]. In amorphous polymers three different relaxation processes can occur, which includes, α , β , and γ with increasing frequency [40]. In this study, a part of right wing of α relaxation map which nullifies around 10 Hz and a β relaxation peak was observed at around 10^3 Hz (Fig. 16) with both virgin and gamma-irradiated epoxy resin materials.

Further, with the increase in the temperature, the real relative permittivity and loss tangent of both virgin and gamma-irradiated specimens were found to be increased. Smaoui *et al.* have indicated that, the dielectric permittivity and dielectric loss factor of epoxy-based polymeric material, become strongly dependent on the temperature at lower frequencies and reach higher values at high temperatures, due to DC conductivity effect [41]. Similar characteristics are observed here, with the epoxy specimens having higher rate of increase in permittivity and loss tangent values with respect to temperature, at lower frequencies compared to higher frequencies. The real relative permittivity and dielectric loss tangent of gamma-ray-irradiated specimens are found to be marginally higher when compared to the virgin specimen. At low frequencies ($<10 \text{ Hz}$) and high temperatures ($>50^\circ\text{C}$), the increase in real relative permittivity with increase in radiation dosage is found to be significant (Fig. 16). The rise in the real relative permittivity at lower frequencies, with respect to gamma-ray irradiation, may be attributed to the radiation-induced chemical reactions can alter the material structure. The radiation energy ionises the molecule resulting in the formation of an ion pair. It can cause a rupture in the side branch or in the main chain, which creates energetic free radicals (small molecules) that are ready to induce a series of chemical reactions through mechanisms like chain scission, oxidation and cross-linking. The chain scission and oxidation reactions result in the formation of small molecules or polar groups. For epoxy resin, polar groups like carbonyl group ($\text{C}=\text{O}$) and hydroxyl group ($-\text{OH}$) were reported as reaction products by oxidation reaction [42]. As a result of these smaller polar molecules, the dipole orientation will be more and the permittivity will be enhanced.

To describe the dielectric behaviour of virgin and gamma-irradiated epoxy nanocomposites, the real relative permittivity (ϵ') and imaginary relative permittivity (ϵ'') were modelled using Cole-Cole double relaxation model [43]. The first term in (6) represents

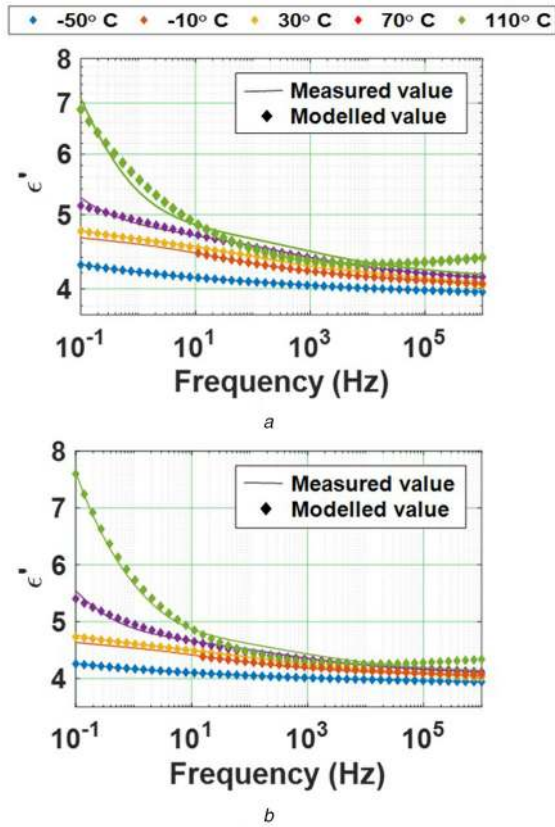


Fig. 17 Measured and modelled ϵ' values of (a) Virgin and, (b) 8 kGy gamma irradiated specimens

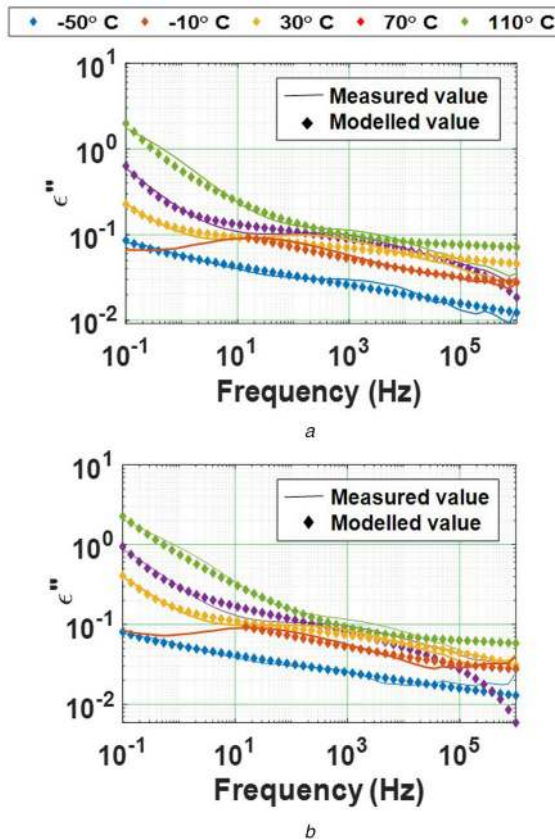


Fig. 18 Measured and modelled ϵ'' values of (a) Virgin and, (b) 8 kGy gamma irradiated specimens

relative permittivity at very high frequencies (ϵ_∞), second term represents the inverse power law dependence of permittivity on frequency ($A\omega^{-n}$) and the remaining part represents the real part of

Cole-Cole expressions with two distinct relaxation times τ_1 and τ_2 . The imaginary part of the complex permittivity ϵ'' , as shown in (7) was calculated by the addition of DC losses to Kramers Kronig (K-K) transformation of (6) [43].

$$\epsilon' = \epsilon_\infty + A\omega^{-n} + \text{Re} \left[\frac{\Delta\epsilon_1}{1 + (j\omega\tau_1)^{1-\alpha_1}} + \frac{\Delta\epsilon_2}{1 + (j\omega\tau_2)^{1-\alpha_2}} \right] \quad (6)$$

$$\epsilon'' = \frac{\sigma_{dc}}{\omega\epsilon_0} + A\omega^{-n} \cot \left(\frac{(1-n)\pi}{2} \right) + \text{Im} \left[\frac{\Delta\epsilon_1}{1 + (j\omega\tau_1)^{1-\alpha_1}} + \frac{\Delta\epsilon_2}{1 + (j\omega\tau_2)^{1-\alpha_2}} \right] \quad (7)$$

where A is the intensity of low frequency dispersion process, $\Delta\epsilon_1$ and $\Delta\epsilon_2$ are the change in permittivity of first and second Cole-Cole process, respectively, α_1 and α_2 are the coefficients of first and second Cole-Cole process, respectively, τ_1 and τ_2 are the relaxation times of first and second Cole-Cole process, respectively. σ_{dc} is the DC conductivity, $\epsilon_0 = 8.85 \times 10^{-12}$ F/m is the permittivity of the free space and $\omega = 2\pi f$ is the angular frequency.

Figs. 17 and 18 depict the measured and modelled ϵ' and ϵ'' values of virgin and gamma irradiated specimens, respectively, as a function of frequency, at different temperatures. Admittedly, in the range of frequency studies, the variation in ϵ'' , especially at -10°C , the model holds good from 10 Hz, where the β relaxation peak occurs. The α -relaxation peak, especially at -10°C , it lies at much lower frequency. Further analysis on this aspect needs to be carried out, as a part of future work. The method of least square technique was used to estimate all the parameters (Table 4) from the (6) and (7). A mean square error margin of 0.0001 has been maintained in order to obtain the best fit to the measured value. Table 5 corresponds to the DC conductivity (σ_{dc}) of test specimens at different temperatures. It is clear that the DC conductivity of the test specimens increases with increase in temperature. It is because of the increase in the mobility of the charge carriers with respect to temperature that led to the increase in the conductivity [44].

Also, there is a marginal increment in the DC conductivity of the epoxy specimens with radiation dose, which could also be due to the increased mobility of the charge carriers after radiation. The activation energy (E_a) is the minimum of energy that is essential to cause a physico-chemical transition in the material, which can be calculated with the help of Arrhenius equation shown in (8) [45].

$$\sigma_{dc} = \sigma_0 e^{-(E_a/K_B T)} \quad (8)$$

where σ_0 is pre-exponential factor, K_B is Boltzmann constant and T is the absolute temperature (in kelvin).

The Arrhenius plot [$\ln(\sigma_{dc})$ versus $(1/T)$] of epoxy specimens is represented in Fig. 19. The calculated activation energies from the Arrhenius plot are tabulated in Table 5. A slight reduction in the activation energy of the epoxy specimens with increase in radiation dose is noticed. Peng *et al.* have stated that the higher activation energy is an indication of the charge carriers being captured in relatively deep traps [44].

Thus the reduction in activation energy with increase in radiation dose is an indication for the charge carriers being trapped in relatively shallow traps, thereby increasing charge carrier mobility. This can be correlated with the increase in the decay rate of average space charge density during depoling, with increment in radiation dose.

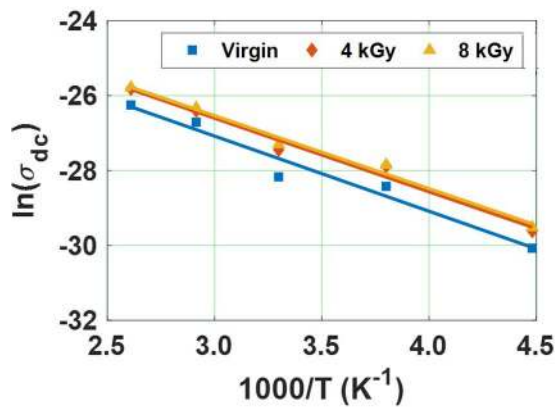
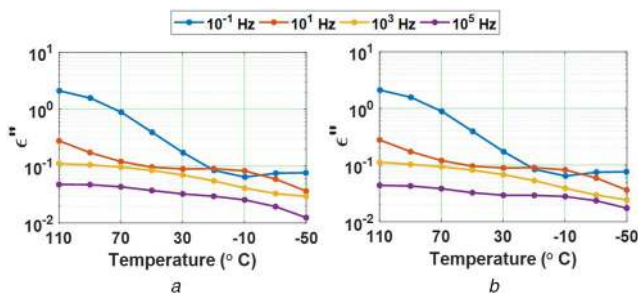
The variation in the imaginary relative permittivity (in logarithmic scale) values of virgin and gamma irradiated specimens with respect to temperature (reversed temperature scale), at different frequencies is represented in Fig. 20. Fréchet *et al.* have indicated the dielectric relaxation map in which α , β , and γ relaxation peaks were represented with decreasing temperature [46]. The right wing of α relaxation peak is more significantly visible for the frequency of 0.1 Hz, in case of all the test specimens. In the measured range of temperatures, a broad β

Table 4 Estimated model parameters for the dielectric responses of the test specimens at different temperatures

Parameters	-50°C		-10°C		30°C		70°C		110°C	
	virgin	8 kGy	virgin	8 kGy	virgin	8 kGy	virgin	8 kGy	virgin	8 kGy
A	0.338	0.337	0.786	0.786	1.29	1.09	1.26	1.24	2.59	2.55
N	0.110	0.093	0.133	0.133	0.059	0.092	0.095	0.177	0.332	0.272
ϵ_1	0.233	2.29	2.08	2.07	4.40	4.96	23.9	27.4	18.4	191
τ_1	10.0	10.0	9.49×10^{-5}	1.07×10^{-4}	37.6	47.6	83.1	84.3	136	177
α_1	1.0	0.996	0.906	0.907	0.999	0.985	0.958	0.953	0.949	0.949
ϵ_2	3.45	3.41	4.14	4.13	0.804	1.39	14.4	16.3	150	148
τ_2	3.80	3.77	4.22×10^{-6}	5.34×10^{-6}	0.012	1.84×10^{-7}	0.036	0.038	0.452	0.086
α_2	1.00	1.00	1.00	1.00	1.00	1.00	0.932	0.924	0.941	0.939
$\sigma (\times 10^{-13})$	0.87	1.52	4.53	8.02	5.84	13.9	25.1	36.9	39.7	63.4

Table 5 DC conductivity and activation energy of epoxy specimens

Sample	DC Conductivity ($\times 10^{-13}$ S/m)					Activation energy, eV
	-50°C	-10°C	30°C	70°C	110°C	
Virgin	0.87	4.53	5.84	25.1	39.7	0.173
4 kGy	1.38	5.62	13.2	34.4	61.6	0.169
8 kGy	1.52	7.79	13.9	36.9	63.4	0.168

**Fig. 19** Arrhenius plot of test specimens**Fig. 20** Temperature variation in ϵ'' values of (a) Virgin and, (b) 8 kGy gamma irradiated specimens

relaxation is seen around -10°C , for the frequency of 10 Hz. This β relaxation consists of shorter relaxation time, less magnitude of relaxation peak and can be attributed to the crankshaft motions of the hydroxyl-ether groups located along the molecular chains [46].

3.4 Elemental analysis and hardness calculation by LIBS

Fig. 21 shows the emission spectra of test samples. In the emission spectra of epoxy specimens, few peaks of Zr along with Si and O are identified with the help of the NIST database. This could be due to the presence of zirconium in the ion trapping particle (IXE). It is observed that there is no change in the elemental composition of the epoxy nano-micro composites after gamma irradiation, but there is a slight reduction in the intensity of the emission spectra.

The plasma temperature can be calculated using the Boltzmann-Saha equation shown in the following equation:

$$T_e = 1.44 \frac{E_2 - E_1}{\ln(I_1 \lambda_1 A_2 g_2 / I_2 \lambda_2 A_1 g_1)} \quad (9)$$

where E_1 and E_2 are energies of excited energy levels 1 and 2, respectively, g_1 and g_2 are statistical weights, A_1 and A_2 are transition probabilities of states, I_1 and I_2 are intensities of particular atomic species at λ_1 and λ_2 wavelength, respectively, and T_e is the plasma electron temperature under the local thermodynamic equilibrium.

Tables 6 and 7 show the plasma temperature, micro Vickers hardness and crater depth values of test specimens. In each sample, the zirconium peaks were used to calculate the plasma temperature. It was observed that the plasma temperatures were decreasing as the dosage of gamma radiation increases. The crater depth of the samples formed after hitting the surface of the insulating material with 15 laser pulses with a time interval of 1 s between each hit, increases with dosage amount of the radiation. The depth of the crater formed was measured by using a non-contact profilometer. Vickers hardness number (HV) and is calculated as [47]:

$$\text{HV} = 1.8544 * \left(\frac{F}{d^2} \right) \text{ kgf/mm}^2 \quad (10)$$

where d is the average of the two diagonals of the imprint formed by indenter and F is the applied load.

It is observed that the Vickers hardness of the samples, calculated from Vickers hardness test, follows the same pattern of plasma temperature of the samples (Table 6). The intensity ratio calculated between the ionic line and the atomic spectral line of zirconium is found to have a direct correlation with the Vickers hardness of the specimen (Table 7). Cowpe *et al.* in [48] observed that the plasma temperature of the bio-ceramic sample increases with increasing hardness of the sample. Abdel-Salam *et al.* [49] stated that the Vickers hardness number of human teeth, shellfish, and eggshells are proportional to the intensity ratios between the ion line and the atomic line for calcium and magnesium in the plasma spectrum. From Tables 6 and 7, it is observed that the calculations of plasma temperature and ion line to atomic line intensity ratio are indirect and non-intrusive methods for estimating the hardness of the material. The plasma electron density was estimated using the following equation:

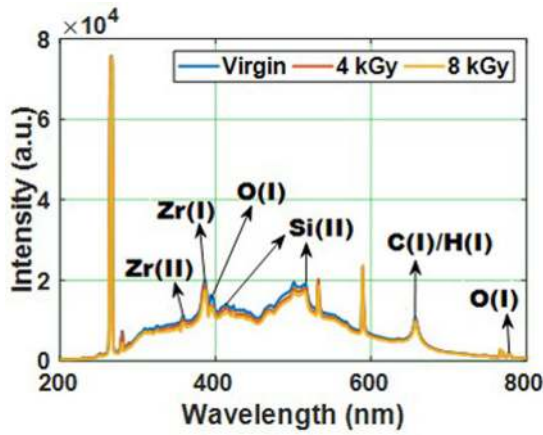


Fig. 21 Emission spectra of virgin and gamma irradiated epoxy nano-micro composites

Table 6 Plasma temperature and Vickers hardness, of test specimens

Specimens	Plasma temperature, K	Vickers hardness number
Virgin	9611.0	53.38 ± 0.98
4 kGy	9482.0	50.08 ± 1.36
8 kGy	9413.6	49.65 ± 1.68

Table 7 Crater depth, electron density and intensity ratio of test specimens

Specimens	Crater depth, μm	Electron density (× 10 ²² cm ⁻³)	Intensity ratio
Virgin	74.01 ± 8.69	1.0612	0.4834
4 kGy	85.38 ± 12.43	1.0836	0.4734
8 kGy	86.15 ± 12.25	1.0994	0.4666

$$n_e = 6.6 \times 10^{21} \frac{I_a A_i g_i}{I_i A_a g_a} \exp\left(-\frac{E^{\text{ion}} + E_i - E_a}{T}\right) \quad (11)$$

where E_i and E_a are energies of excited energy levels of ionic and atomic species, respectively, g_i and g_a are statistical weights, A_i and A_a are transition probabilities of states, I_i and I_a are intensities of particular ionic and atomic species at λ_1 and λ_2 wavelengths, respectively, E^{ion} is the ionisation energy and n_e is the plasma electron density under the local thermodynamic equilibrium.

The plasma electron density of the test specimens is calculated from the ion line (Zr II) and atomic spectral line (Zr I) of zirconium and is represented in Table 7. It is observed that the plasma electron density of the test specimens increases with increase in dosage of radiation.

4 Conclusions

The important conclusions accrued based on this study are the following:

- Presence of homo-charge due to charge injection has been observed in the space charge profile of both virgin and gamma-irradiated epoxy micro-nano composites. This charge injection is found to increase with increase in the magnitude of DC electric field applied.
- The threshold of space charge accumulation (E_T) is found to be reduced and the rate of space charge accumulation (b) is found to be increased with an increase in dosage of gamma irradiation.
- It is observed that the average space charge density during poling and charge decay rate during depoling, under 10 kV/mm positive DC field, is higher for gamma-irradiated specimens when compared with the virgin specimen.

- Space charge measurements made during voltage polarity reversal indicated that a part of the homo-charge injected from electrodes, remained as hetero-charge just after polarity reversal and could result in the distortion of the electric field.
- The initial surface potential has a marginal reduction with an increase in the dosage of gamma radiation, but the surface potential decay rate has increased significantly.
- A left shift in the peak value of the trap distribution characteristics is observed with an increase in the dosage of gamma radiation. It indicates the reduction in the trap depth which further indicates the presence of shallow traps and increase in charge mobility after irradiation.
- It is observed that the real relative permittivity decreases with increase in frequency and increases with increase in temperature. A marginal increase in relative permittivity and dielectric loss tangent is noticed with an increase in dosage of gamma radiation.
- The DC conductivity is found to be increased with increase in temperature and also with radiation dose. It is also observed that the activation energy of the epoxy specimens, reduces with an increase in radiation dose.
- LIBS reflected no change in elemental composition when subjected to gamma irradiation. The variation in plasma temperature and ion line to atomic line intensity ratio with dosage of gamma radiation is proportional to the Vickers hardness number of the specimens, thereby forming an indirect method for the estimation of hardness of the material with respect to ageing.
- The presence of zirconium content in epoxy micro-nano composites due to IXE compound, has increased the hardness of the material.

In short, it could be concluded that the gamma irradiation of epoxy nano-micro composites have a high impact on space charge and charge trap characteristics of the material along with a reduction in permittivity and hardness of the material.

5 References

- [1] Tanaka, T., Imai, T.: 'Advanced nanodielectrics: fundamentals and applications' (CRC Press, United States, 2017)
- [2] Luo, P., Xu, M., Wang, S., et al.: 'Structural, dynamic mechanical and dielectric properties of mesoporous silica/epoxy resin nanocomposites', *IEEE Trans. Dielectr. Electr. Insul.*, 2017, **24**, (3), pp. 1685–1697
- [3] Du, B.X., Guo, Y.G.: 'Tracking resistance of epoxy/Al₂O₃ nanocomposites under DC voltage', *IEEE Trans. Dielectr. Electr. Insul.*, 2015, **22**, (1), pp. 109–116
- [4] Qiang, D., Wang, Y., Chen, G., et al.: 'Dielectric properties of epoxy silica and boron nitride nanocomposites and moisture/temperature influences', *IET Nanodielectrics*, 2018, **1**, (1), pp. 48–59
- [5] Sun, W., Bowler, N.: 'Dielectric properties of silanized-silicon/epoxy nanocomposites', *IEEE Trans. Dielectr. Electr. Insul.*, 2016, **23**, (4), pp. 2095–2101
- [6] Dai, S., Zhang, T., Mo, S., et al.: 'Study on preparation, thermal conductivity, and electrical insulation properties of epoxy/AIN', *IEEE Trans. Appl. Super Cond.*, 2019, **29**, (2), pp. 1–6
- [7] Heid, T., Fréchette, M., David, E.: 'Epoxy/BN micro-and submicro-composites: dielectric and thermal properties of enhanced materials for high voltage insulation systems', *IEEE Trans. Dielectr. Electr. Insul.*, 2015, **22**, (2), pp. 1176–1185
- [8] Du, B.X., Liang, H.C., Li, J., et al.: 'Temperature dependent surface potential decay and flashover characteristics of epoxy/SiC composites', *IEEE Trans. Dielectr. Electr. Insul.*, 2018, **25**, (2), pp. 631–638
- [9] Liang, M., Wong, K.L.: 'Improving the long-term performance of composite insulators use nanocomposite: a review', *Energy Proc.*, 2017, **110**, pp. 168–173
- [10] Huang, K.S., Nien, Y.H., Chen, J.S., et al.: 'Synthesis and properties of epoxy/TiO₂ composite materials', *Polym. Compos.*, 2006, **27**, (2), pp. 195–200
- [11] Saha, D., Anisimov, A.G., Groves, R.M., et al.: 'Epoxy-hBN nanocomposites: a study on space charge behavior and effects upon material', *IEEE Trans. Dielectr. Electr. Insul.*, 2017, **24**, (3), pp. 1718–1725
- [12] Tsekmes, I.A., Morshuis, P.H.F., Smit, J.J., et al.: 'Enhancing the thermal and electrical performance of epoxy micro composites with the addition of nanofillers', *IEEE Electr. Insul. Mag.*, 2015, **31**, (3), pp. 32–42
- [13] Abdelkader, K., Pascal, R., Olivier, L., et al.: 'Dielectric relaxation and ionic conduction in 66% Silica/CW229-3/HW229-1 microcomposite', *Polym. Compos. B: Eng.*, 2015, **78**, pp. 488–496
- [14] Imai, T., Sawa, F., Nakano, T., et al.: 'Effects of nano-and micro-filler mixture on electrical insulation properties of epoxy based composites', *IEEE Trans. Dielectr. Electr. Insul.*, 2006, **13**, (2), pp. 319–326

- [15] Mishra, P., Desai, B.M.A., Vasa, N.J., *et al.*: 'Understanding the performance of gamma-ray-irradiated epoxy nanocomposites', *Micro Nano Lett.*, 2019, **14**, (1), pp. 107–112
- [16] Kraus, K.A., Phillips, H.O.: 'Adsorption on inorganic materials I. Cation exchange properties of zirconium phosphate', *J. Am. Chem. Soc.*, 1956, **78**, (3), pp. 694–694
- [17] Du, B.X., Xiao, M.: 'Influence of surface charge on DC flashover characteristics of epoxy/BN nanocomposites', *IEEE Trans. Dielectr. Electr. Insul.*, 2014, **21**, (2), pp. 529–536
- [18] Llovera, P., Molinie, P.: 'New methodology for surface potential decay measurements: application to study charge injection dynamics on polypropylene films', *IEEE Trans. Dielectr. Electr. Insul.*, 2004, **11**, (6), pp. 1049–1056
- [19] Du, B.X., Li, A.: 'Effects of DC and pulse voltage combination on surface charge dynamic behaviors of epoxy resin', *IEEE Trans. Dielectr. Electr. Insul.*, 2017, **24**, (4), pp. 2025–2033
- [20] Dong, J., Shao, Z., Wang, Y., *et al.*: 'Effect of temperature gradient on space charge behavior in epoxy resin and its nanocomposites', *IEEE Trans. Dielectr. Electr. Insul.*, 2017, **24**, (3), pp. 1537–1546
- [21] Qiang, D., Wang, Y., Wang, X., *et al.*: 'The effect of filler loading ratios and moisture on DC conductivity and space charge behaviour of SiO₂ and hBN filled epoxy nanocomposites', *J. Phys. D: Appl. Phys.*, 2019, **52**, (39), p. 395502
- [22] Das, S., Gupta, N.: 'Effect of ageing on space charge distribution in homogeneous and composite dielectrics', *IEEE Trans. Dielectr. Electr. Insul.*, 2015, **22**, (1), pp. 541–547
- [23] Chen, G., Davies, A.E., Banford, H.M.: 'Influence of radiation environments on space charge formation in gamma-irradiated LDPE', *IEEE Trans. Dielectr. Electr. Insul.*, 1999, **6**, (6), pp. 882–886
- [24] Chen, G., Hao, M., Xu, Z., *et al.*: 'Review of high voltage direct current cables', *CSEE J. Power Energy Syst.*, 2015, **1**, (2), pp. 9–21
- [25] Laghari, J.R., Hammoud, A.N.: 'A brief survey of radiation effects on polymer dielectric', *IEEE Trans. Nucl. Sci.*, 1990, **37**, (2), pp. 1076–1083
- [26] Wang, X., Hong, X., Chen, P., *et al.*: 'Surface hardness analysis of aged composite insulators via Laser-induced plasma Spectra characterization', *IEEE Trans. Plasma Sci.*, 2018, **47**, (1), pp. 387–394
- [27] Zhang, S., Wang, X., He, M., *et al.*: 'Laser-induced plasma temperature', *Spectrochim. Acta, Part B*, 2014, **97**, pp. 13–33
- [28] Aberkane, S.M., Bendib, A., Yahiaoui, K., *et al.*: 'Correlation between Fe–V–C alloys surface hardness and plasma temperature via LIBS technique', *Appl. Surf. Sci.*, 2014, **301**, pp. 225–229
- [29] Montanari, G.C., Fabiani, D.: 'Evaluation of dc insulation performance based on space-charge measurements and accelerated life tests', *IEEE Trans. Dielectr. Electr. Insul.*, 2000, **7**, (3), pp. 322–328
- [30] Alijagic-Jonuz, B.: 'Dielectric properties and space charge dynamics of polymeric high voltage DC insulating materials', PhD thesis, TU Delft, Delft University Press, 2007
- [31] Chen, G., Fu, M.: 'The influence of gamma irradiation on space charge in LDPE'. IEEE 8th Int. Conf. on Properties & applications of Dielectric Materials, Bali, Indonesia, 2006, pp. 131–134
- [32] Wang, S., Luo, S., Tu, Y., *et al.*: 'Effect of polarity reversal on space charge properties of CB/LDPE composite under DC field', *IEEE Trans. Dielectr. Electr. Insul.*, 2017, **24**, (3), pp. 1349–1354
- [33] Liu, P., Ning, X., Peng, Z., *et al.*: 'Effect of temperature on space charge characteristics in epoxy resin', *IEEE Trans. Dielectr. Electr. Insul.*, 2015, **22**, (1), pp. 65–71
- [34] Gao, Y., Du, B.X.: 'Effect of gamma-ray irradiation on surface charge accumulation of epoxy resin', *Polym. Mater. Sci. Eng.*, 2012, **28**, (11), pp. 815–825
- [35] Simmons, J.G., Tam, M.C.: 'Theory of isothermal currents and the direct determination of trap parameters in semiconductors and insulators containing arbitrary trap distributions', *Phys. Rev. B*, 1973, **7**, (8), pp. 3706–3713
- [36] Watson, P.K.: 'The thermalization and trapping of electrons in polystyrene', *IEEE Trans. Electr. Insul.*, 1987, **2**, pp. 129–132
- [37] Ishimoto, K., Kanegae, E., Ohki, Y., *et al.*: 'Superiority of dielectric properties of LDPE/MgO nanocomposites over microcomposites', *IEEE Trans. Dielectr. Electr. Insul.*, 2009, **16**, (6), pp. 1735–1742
- [38] Singha, S., Thomas, M.J.: 'Dielectric properties of epoxy nanocomposites', *IEEE Trans. Dielectr. Electr. Insul.*, 2008, **15**, (1), pp. 12–23
- [39] Baziard, Y., Breton, S., Toutain, S., *et al.*: 'Dielectric properties of aluminium powder-epoxy resin composites', *Eur. Polym. J.*, 1988, **24**, (6), pp. 521–526
- [40] Couderc, H., Fréchette, M., Savoie, S., *et al.*: 'Dielectric and thermal properties of boron nitride and Silica epoxy composites'. IEEE Int. Symp. on Electrical Insulation, San Juan, 2012, pp. 64–68
- [41] Smaoui, H., Arous, M., Guermazi, H., *et al.*: 'Study of relaxations in epoxy polymer by thermally stimulated depolarization current (TSDC) and dielectric relaxation spectroscopy (DRS)', *J. Alloy Compd.*, 2010, **489**, (2), pp. 429–436
- [42] Gao, Y., Du, B.X.: 'Effect of Gamma-ray irradiation on permittivity and dielectric loss of polymer insulating materials'. Int. Conf. on High Voltage Engineering and Application, Shanghai, 2012, pp. 229–232
- [43] Jonscher, A. K.: '*Dielectric relaxation in solids*' (London, UK, Chelsea Dielectrics Press Limited, 1996, 2nd Edn.)
- [44] Peng, W., Huang, X., Yu, J., *et al.*: 'Electrical and thermo-physical properties of epoxy/aluminum nitride nanocomposites: effects of nanoparticle surface modification', *Compos. A: Appl. Sci. Manuf.*, 2010, **41**, (9), pp. 1201–1209
- [45] Wang, Z., Zhou, W., Dong, L., *et al.*: 'Dielectric spectroscopy characterization of relaxation process in Ni/epoxy composites', *J. Alloys Compd.*, 2016, **682**, pp. 738–745
- [46] Fréchette, M., Preda, I., Castellon, J., *et al.*: 'Polymer composites with a large nanofiller content: a case study involving epoxy', *IEEE Trans. Dielectr. Electr. Insul.*, 2014, **21**, (2), pp. 434–443
- [47] Meyers, M.A., Chawla, K.K.: '*Mechanical behavior of materials*' (Cambridge University Press, Cambridge, UK, 2008)
- [48] Cowpe, J.S., Moorehead, R.D., Moser, D., *et al.*: 'Hardness determination of bio-ceramics using laser-induced breakdown spectroscopy', *Spectrochim. Acta, Part B*, 2011, **66**, (3–4), pp. 290–294
- [49] Abdel-Salam, Z.A., Galmed, A.H., Tognoni, E., *et al.*: 'Estimation of calcified tissues hardness via calcium and magnesium ionic to atomic line intensity ratio in laser induced breakdown spectra', *Spectrochim. Acta, Part B*, 2007, **62**, (12), pp. 1343–1347